

measurements. We argue that SML is initiated by modes at these frequencies through the Kerr-lens mechanism described above; once they are locked in phase, their mutual beating produces a large enough modulation of the laser gain to bring several other modes above threshold.

References and Notes

1. W. Kaiser, Ed., *Ultrashort Laser Pulses: Generation and Applications*, vol. 60 of *Topics in Applied Physics Series* (Springer-Verlag, Berlin, 1993).
2. T. Elsaesser, J. G. Fujimoto, D. A. Wiersma, W. Zinth, Eds., *Ultrafast Phenomena XI* (Springer-Verlag, Berlin, 1998).
3. G. Steinmeyer, D. H. Sutter, L. Gallmann, N. N. Matuschek, U. Keller, *Science* **286**, 1507 (1999).
4. Present sources include mode-locked and gain-switched CO₂ lasers [see, for instance, I. V. Pogorelsky et al., *IEEE J. Quantum Electron.* **31**, 556 (1995)], limited to $\lambda \approx 10.6 \mu\text{m}$, and picosecond and femtosecond optical parametric oscillators [for a review, see M. H. Dunn, M. Ebrahimzadeh, *Science* **286**, 1513 (1999)], which however are still rather complex sources. Recently, we have obtained picosecond midinfrared pulses with QC lasers, including gain-switching [R. Paiella et al., *Appl. Phys. Lett.* **75**, 2536 (1999)] and active mode-locking [R. Paiella et al., *Appl. Phys. Lett.* **77**, 169 (2000)].
5. J. Faist et al., *Science* **264**, 553 (1994).
6. F. Capasso et al., *Opt. Photonics News* **10**, 31 (1999).
7. M. M. Fejer, S. J. B. Yoo, R. L. Byer, A. Harwit, J. S. Harris, *Phys. Rev. Lett.* **62**, 1041 (1989).
8. M. Segev, I. Grave, A. Yariv, *Appl. Phys. Lett.* **61**, 2403 (1992).
9. F. Capasso, C. Sirtori, A. Y. Cho, *IEEE J. Quantum Electron.* **30**, 1313 (1994).
10. E. Rosencher et al., *Science* **271**, 168 (1996).
11. A. Neogi, H. Yoshida, T. Mozume, O. Wada, *J. Appl. Phys.* **85**, 3352 (1999).
12. R. W. Boyd, *Nonlinear Optics* (Academic Press, San Diego, CA, 1992).
13. J. Faist et al., *IEEE J. Quantum Electron.* **34**, 336 (1998).
14. C. Gmachl et al., *IEEE J. Select. Topics Quantum Electron.* **5**, 808 (1999).
15. Although room temperature operation of QC lasers is readily achieved in pulsed mode, continuous-wave operation is at present limited to temperatures below 175 K.
16. H. C. Liu, J. Li, M. Buchanan, Z. R. Wasilewski, *IEEE J. Quantum Electron.* **32**, 1024 (1996). These detectors are also based on intersubband transitions in semiconductor quantum wells, and therefore they are very well suited for high-speed applications. The device used here has a nominal bandwidth of 12 GHz (parasitics limited).
17. For a general review of QWIPs, see B. F. Levine, *J. Appl. Phys.* **74**, R1 (1993).
18. P. R. Griffiths, J. A. de Haseth, *Fourier Transform Infrared Spectrometry* (Wiley, New York, 1986).
19. J. F. Martins-Filho, E. A. Avrutin, C. N. Ironside, J. S. Roberts, *IEEE J. Select. Topics Quantum Electron.* **1**, 539 (1995).
20. The decay in the amplitude of the spikes with increasing delay time observed in Fig. 3 is an instrumental effect, resulting from the nonperfect collimation of the beam entering the FTIR, through a mechanism known as self-apodization (18). This is confirmed by the fact that a decay at the same rate is observed in the interferograms for single-mode cw operation of the same lasers. On the other hand, a much faster decay would be observed if the laser modes were not phase-locked to one another (19).
21. G. P. Agrawal, *Nonlinear Fiber Optics* (Academic Press, San Diego, CA, 1995).
22. C. H. Lin, T. K. Gustafson, *IEEE J. Quantum Electron.* **8**, 429 (1972).
23. Surface plasmons are electromagnetic waves propagating at the interface between two materials with dielectric constants having real parts of opposite sign, such as a metal and an insulator. For more details,

see, for instance, P. Yeh, *Optical Waves in Layered Media* (Wiley, New York, 1988).

24. A. Yariv, *Quantum Electronics* (Wiley, New York, 1988).
25. D. E. Spence, P. N. Kean, W. Sibbett, *Opt. Lett.* **16**, 42 (1991).
26. G. P. Agrawal, N. K. Dutta, *Long-Wavelength Semiconductor Lasers* (Van Nostrand Reinhold, New York, 1986).
27. The following parameter values, corresponding to the laser of Fig. 1, were used in the computation of $n_{z_2}z_{32} = 1.9 \text{ nm}$ (theoretical); $\Delta\nu = 3 \text{ THz}$ (measured from electroluminescence spectra in similar devices); $n_0 = 3.3$ (measured from the mode separation frequency); $\Delta N = (I_{\text{el}}\tau_3)/(qV) = 8 \times 10^{15} \text{ cm}^{-3}$, with

the carrier lifetime $\tau_3 = 1.5 \text{ ps}$ (theoretical), the volume of one period of active region $V = 677 \mu\text{m}^3$, at a current $I_{\text{el}} = 0.6 \text{ A}$ (corresponding to the second trace from top in Fig. 1); and $I_0^{\text{sat}} = (\hbar^2\epsilon_0cn\Delta\nu)/(8\pi\Gamma q^2z_{32}^2\tau_3) = 1.4 \text{ MW/cm}^2$, with the active-layers confinement factor $\Gamma = 23\%$. Finally, ϕ_{max} was computed with Eq. 2 with $I_{\text{max}} = 5.5 \text{ MW/cm}^2$ (inferred from the measured average power at a current of 0.6 A).

28. We thank H. Y. Hwang, A. M. Sergent, and E. Chaban for technical assistance and M. C. Wanke, R. Colombelli, and A. Tredicucci for stimulating discussions. Supported in part by Defense Advanced Research Projects Agency/U.S. Army Research Office under contract DAAD19-00-C-0096.

27 July 2000; accepted 19 October 2000

Tunable Resistance of a Carbon Nanotube–Graphite Interface

S. Paulson,^{1*} A. Helser,² M. Buongiorno Nardelli,³
R. M. Taylor II,^{2,1} M. Falvo,^{1†} R. Superfine,¹ S. Washburn¹

The transfer of electrons from one material to another is usually described in terms of energy conservation, with no attention being paid to momentum conservation. Here we present results on the junction resistance between a carbon nanotube and a graphite substrate and show that details of momentum conservation also can change the contact resistance. By changing the angular alignment of the atomic lattices, we found that contact resistance varied by more than an order of magnitude in a controlled and reproducible fashion, indicating that momentum conservation, in addition to energy conservation, can dictate the junction resistance in graphene systems such as carbon nanotube junctions and devices.

The engineering of electronic devices relies on the control and exploitation of the electronic properties of junctions. The density of states of the two materials as a function of energy is typically used to describe these properties. New opportunities arise when the momentum transfer across the junction can be controlled. Carbon nanotubes (NTs) offer a laboratory for this control because they have a highly structured Fermi surface that restricts the allowed momentum states available at the junction (1–3) and have atomically smooth lattices at the contact region. The molecular size and mechanical and electronic properties of NTs have made them prime targets as components of nanometer-sized electronic and actuating devices (4–8). Experimental studies of devices that include both metal-NT and NT-NT junctions have demonstrated that the control of contact resistance will be essential for predictable device specifications (9, 10) and that it remains

an elusive goal. Here we present measurements of a multiwalled NT (MWNT) in contact with a graphite [highly oriented pyrolytic graphite (HOPG)] substrate; these materials have similar energy dispersions and available momentum states. The modulation in the electrical resistance of the contact we observed demonstrates the importance of lattice registry in NT/NT devices and opportunities for sensing and actuating device designs (11).

We measured the resistance of a MWNT-HOPG contact as a function of the rotation angle of the atomic lattices. Measurements were made with a two-probe technique (Fig. 1A); the HOPG substrate itself served as one lead, and a conducting atomic force microscope (AFM) tip brought into contact with the top of the NT was the other. After 200 μl of a MWNT/dichloromethane suspension was dispensed onto the rapidly spinning HOPG substrate, the sample was rinsed with ethanol, cleaned by exposure to ultraviolet light, and rinsed in water. The NT was imaged in noncontact (oscillating) mode to identify its position; then in contact mode, it was pushed, causing it to rotate (and translate) on the graphite plane until the commensurate, or in-registry, position was found, as evidenced by a sharp increase in lateral force (12). This position is designated as $\Phi = 0^\circ$. Schematics of NTs in registry at $\Phi = 0^\circ$ (Fig. 1B) and out of registry at $\Phi = 10^\circ$ (Fig. 1C)

¹Department of Physics and Astronomy, ²Department of Computer Science, University of North Carolina–Chapel Hill, Chapel Hill, NC 27599, USA. ³Department of Physics, North Carolina State University, Raleigh, NC 27695–8202, USA.

*Present address: Department of Physics and Center for Nonlinear and Complex Systems, Duke University, Durham, NC 27708, USA.

†To whom correspondence should be addressed. E-mail: falvo@physics.unc.edu

REPORTS

on a graphene sheet are shown. The AFM tip was then engaged in contact mode on top of the MWNT with the desired force (~ 50 nN), and the voltage between the tip and sample was swept through ± 0.1 or 0.25 V while the current was measured. Almost all current-voltage (I - V) curves were linear over the entire range; attempts with larger voltages (~ 1 V) damaged the metal coating of our tip. After the I - V curve, the tip was moved perpendicular to the tube axis, and topographic data were used to determine that the tip had been on the top of the tube; otherwise, the measurement was discarded. The MWNT was nudged into a new position, and the measurement process was repeated.

Data from a MWNT (700 nm long by 30 nm in diameter) that had been rotated through 180° , with resistance measurements taken approximately every 7° to 10° , are shown (Fig. 2A). Similar data have been collected from four other NTs, ranging from 9 to 46 nm in diameter. The resistance minima occur at the in-registry positions $\Phi = 0^\circ, 60^\circ, 120^\circ,$ and 180° ; the maxima occur at orientations displaced 30° ; and the data have a sixfold symmetry, reflecting the symmetry of the lattices. More dense data from a different NT (1.6 μm by 46 nm) are also shown (Fig. 2B). In lateral force measurements taken during the in-plane rotation of an NT (inset to Fig. 2A), the effect of the lattice registry was striking: The force for rotation was constant for all measured angles between the in-registry positions and had a large spike at the lock-in angle (12). In contrast, we observed that the resistance varied continuously as a function of angle, even through the lock-in orientation.

We were interested primarily in the change in resistance of the interface, R_{int} , as the MWNT was rotated. For the data in Fig. 2B, the in-registry two-probe resistance measurement was 4 kilohm and the 30° out-of-registry measurements were 48 kilohm. The ratio of the interfacial resistances is certainly larger, because our two-terminal resistance $R = R_L + R_{\text{t-NT}} + R_{\text{NT}} + R_{\text{int}}$ includes serial contributions from the leads, R_L ; the tip-NT junction, $R_{\text{t-NT}}$; and the NT itself, R_{NT} . We determined the other contributions to infer R_{int} . Placing the AFM tip directly on the graphite substrate yields a value of 2.7 kilohm. This measurement includes both R_L and $R_{\text{t-NT}}$, assuming that this contact is similar to the tip-NT contact.

We can also estimate the resistance of the NT, R_{NT} . If we assume diffusive transport (13, 14) through the outer shell only (15, 16) and use the literature value for the in-plane resistivity of graphite (17), we obtain a resistance of ~ 300 ohm. This model predicts a resistivity of 4 to 18 kilohm/ μm (depending on the diameter), which compares favorably

with the values of 4 to 10 kilohm/ μm that other groups have observed in arc-discharge-grown NTs (9, 14). Assuming instead that transport in the NT is ballistic (16), each 0.36-nm width (the Fermi wavelength in graphite) of the NT contributes a channel resistance of 13 kilohm. For our tip and tube shape, we expect about 200 ohm (60 channels). Either model predicts that R_{NT} is approximately 300 ohm, and thus the contributions other than R_{int} sum to 3 kilohm. We attribute the remaining 1 kilohm of the in-registry measurement to this interface. At 30° out of registry, the contribution is approximately 45 kilohm. When rotated through an angle of 30° , the resistance of the interface changes by over a factor of 40, indicating that subtle atomic scale differences can have dramatic effects on the contacts to carbon NTs.

We can explain this modulation in terms of the overlap of the momentum states in the two objects. The Fermi surfaces of both graphite (18) and NTs (4) are a set of discrete points. As a consequence in our experiment, allowed momentum states (at low bias) in the NT overlap those in the graphite only near orientations in which the Fermi wave vectors are parallel; that is, the commensurate orientations. The functional form of $R(\Phi)$ will depend on the relaxation of the momentum conservation condition (for example, the size of the contact region and the amount of disorder in the system) and the shape of the Fermi surface [for example, as changed by doping of adsorbed molecules (19, 20) and thermal smearing].

We performed theoretical calculations on a cell containing a 2-nm-long section of

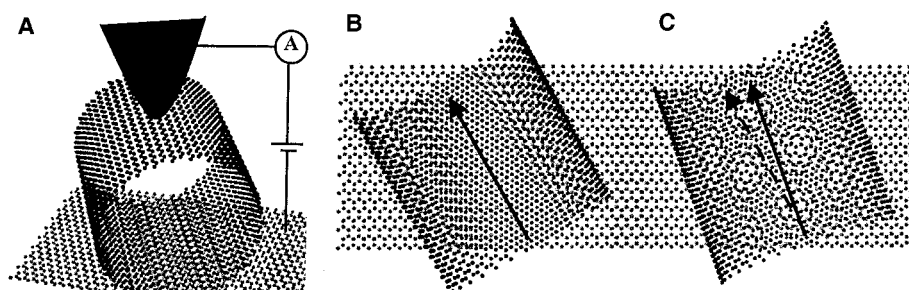
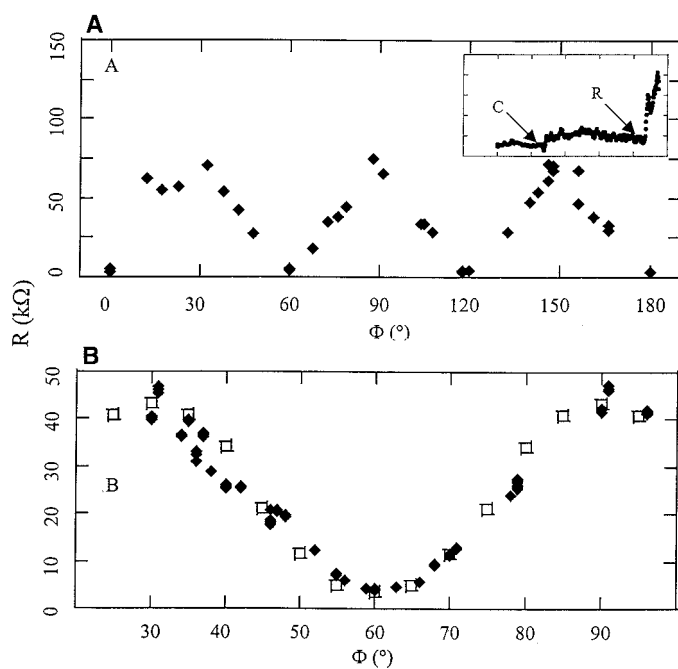


Fig. 1. Schematic of experiment. (A) A conducting AFM tip is used to measure the resistance of the NT-HOPG interface. (B

and C) View of the interface from inside the tube. (B) The NT is in registry, $\Phi = 0^\circ$. Notice the ordered AB stacking of graphite lattices. In this geometry, the electronic wave function of allowed states in the NT (that is, along tube axis) and the graphite (zigzag directions) are parallel. (C) The NT is out of registry, $\Phi = 10^\circ$. The NT Fermi-level states (dotted arrow) are no longer parallel to those in the graphite (solid arrow), and the momentum mismatch causes an increased interface resistance.

Fig. 2. Resistance versus angle for MWNT-HOPG interfaces. (A) A tube that has been rotated through 180° . The resistance is clearly periodic, with minima at the commensurate positions, and increases by a factor of 20 at 30° . (Inset) Lateral force as the AFM tip pushes the NT. At C, the tip contacts the NT, causing it to begin rotating. At R, the NT and graphite are in registry, as indicated by the order-of-magnitude increase in friction; this angle is chosen as $\Phi = 0^\circ$. (B) More dense data over one period on a different tube gives us a better indication of the shape of the curve. We see excellent agreement between experiment (diamonds) and theory (squares).



a (10,10) tube on two layers of graphite. A jellium tip and a lower contact were used to simulate the experimental geometry, and the tip contacted the NT along its entire length. The electronic structure of both the graphite and the tube is described with a simple π -orbital tight binding model. I - V curves were obtained as discussed previously (21) and were fit to the experimental data with a single parameter for the NT-HOPG hopping. Sample calculations were also performed on a MWNT consisting of a (5,5) tube nested inside a (10,10) tube, and no significant differences were observed. The results of our calculations are shown along with the experimental results in Fig. 2B. We found excellent agreement, indicating that the relaxation of the momentum conservation condition (caused here by finite size effects) can account for the angular dependence of $R(\Phi)$. Furthermore, this agreement indicates that our experimental results will scale to single-walled NTs. This is consistent with calculations studying NT-NT contacts (22, 23).

Our results indicate the importance of electron momentum conservation at interfaces, particularly for carbon NTs, where the discrete Fermi surface allows states only in specific directions. Our study implies that the relative angle between the lattices of the NTs can produce dramatic effects, and its control can be exploited in the design of electronic devices and actuating systems.

References and Notes

- P. Delaney, M. Di Ventra, *Appl. Phys. Lett.* **75**, 4028 (1999).
- J. Tersoff, *Appl. Phys. Lett.* **74**, 2122 (1999).
- _____, *Appl. Phys. Lett.* **75**, 4030 (1999).
- J. W. Mintmire, B. I. Dunlap, C. T. White, *Phys. Rev. Lett.* **68**, 631 (1992).
- V. H. Crespi, M. L. Cohen, A. Rubio, *Phys. Rev. Lett.* **79**, 2093 (1997).
- M. Bockrath et al., *Nature* **397**, 598 (1999).
- S. J. Tans, A. R. M. Verschueren, C. Dekker, *Nature* **393**, 49 (1998).
- Z. Yao, H. W. C. Postma, L. Balents, C. Dekker, *Nature* **402**, 273 (1999).
- C. Schonenberger, A. Bachtold, C. Strunk, J. P. Salvetat, L. Forro, *Appl. Phys. A Mat. Sci. Process.* **69**, 283 (1999).
- M. S. Fuhrer et al., *Science* **288**, 494 (2000).
- M. R. Falvo et al., *Nature* **397**, 236 (1999).
- M. R. Falvo, J. Steele, R. M. Taylor II, R. Superfine, *Phys. Rev. B* **62**, 10665 (2000).
- H. Dai, E. W. Wong, C. M. Lieber, *Science* **272**, 523 (1996).
- A. Bachtold et al., *Phys. Rev. Lett.* **84**, 6082 (2000).
- A. Bachtold et al., *Nature* **397**, 673 (1999).
- S. Frank, P. Poncharal, Z. L. Wang, W. A. de Heer, *Science* **280**, 1744 (1998).
- M. S. Dresselhaus, G. Dresselhaus, P. C. Eklund, *Science of Fullerenes and Carbon Nanotubes* (Academic Press, San Diego, CA, 1996).
- P. R. Wallace, *Phys. Rev.* **71**, 622 (1947).
- P. G. Collins, K. Bradley, M. Ishigami, A. Zettl, *Science* **287**, 1801 (2000).
- M. Kruger, M. R. Buitelaar, T. Nussbaumer, C. Schonenberger, preprint available at <http://xxx.lanl.gov/abs/cond-mat/0009171> (2000).
- M. Buongiorno Nardelli, J. Bernholc, *Phys. Rev. B Condens. Matter* **60**, R16338 (1999).
- A. Buldum, J. P. Lu, preprint available at <http://arXiv.org/ftp/cond-mat/papers/0005/0005523.pdf> (2000).
- A. A. Maarouf, C. L. Kane, E. J. Mele, *Phys. Rev. B* **61**, 11156 (2000).
- We are grateful to A. Buldum and J. P. Lu for many useful discussions regarding these experiments as well as their own results. Supported by NSF, the Office of Naval Research–Multidisciplinary Research Program of the University Research Initiative, and NIH–National Center for Research Resources.

15 August 2000; accepted 30 October 2000

Formation of Sphalerite (ZnS) Deposits in Natural Biofilms of Sulfate-Reducing Bacteria

Matthias Labrenz,¹ Gregory K. Druschel,¹ Tamara Thomsen-Ebert,² Benjamin Gilbert,³ Susan A. Welch,¹ Kenneth M. Kemner,⁴ Graham A. Logan,⁵ Roger E. Summons,⁵ Gelsomina De Stasio,³ Philip L. Bond,¹ Barry Lai,⁴ Shelly D. Kelly,⁴ Jillian F. Banfield^{1*}

Abundant, micrometer-scale, spherical aggregates of 2- to 5-nanometer-diameter sphalerite (ZnS) particles formed within natural biofilms dominated by relatively aerotolerant sulfate-reducing bacteria of the family *Desulfobacteriaceae*. The biofilm zinc concentration is about 10^6 times that of associated groundwater (0.09 to 1.1 parts per million zinc). Sphalerite also concentrates arsenic (0.01 weight %) and selenium (0.004 weight %). The almost monomineralic product results from buffering of sulfide concentrations at low values by sphalerite precipitation. These results show how microbes control metal concentrations in groundwater- and wetland-based remediation systems and suggest biological routes for formation of some low-temperature ZnS deposits.

Microbial reduction of sulfate by sulfate-reducing bacteria (SRB) in anoxic environments is the only major source of low-temperature sulfide in natural waters (1). Sulfide can react with metals to form insoluble products (2). Formation of ZnS by SRB under certain laboratory conditions was demonstrated in the 1950s and 1960s (3–5). However, the microbiological, geochemical, and mineralogical interactions leading to ZnS biomineralization in complex natural systems have not been deciphered. Here we report low-temperature, biologically mediated sphalerite precipitation from dilute natural solutions. Microbial precipitation reactions such as those documented here may be central to mine-waste remediation strategies that use natural or artificial wetlands (1, 6). By an analogous process, ancient microorganisms may have contributed to the low-temperature (or early) stages of formation of the large-stratiform sediment-hosted (and other) ZnS ore deposits.

We studied biofilms collected by SCUBA divers from a flooded tunnel within carbonate rocks that host the Piquette Pb-Zn deposit (Tennyson, Wisconsin). Despite the generation of acid due to dissolution of some remaining sulfide ore, the high carbonate-buffering capacity maintains the pH between ~7.2 and 8.6. The water meets drinking-water standards [<5 ppm Zn (7)], and water from nearby wells is used for this purpose (Table 1).

The biofilms are gray [see supplementary material (8)] because they lack ferrihydrite and goethite, which are commonly associated with bacteria in more oxidized regions of the tunnel system (9). Characterization by optical microscopy, scanning electron microscopy (SEM), and transmission electron microscopy (TEM) (8) (Figs. 1 and 2, A to C) revealed that cells are closely associated with spherical mineral aggregates up to 10 μm in diameter (8). Energy dispersive x-ray (Fig. 2D), synchrotron-based x-ray photoelectron emission microscopy (PEEM), and x-ray microprobe analyses (8) show that aggregates contain abundant Zn and S. Selected area electron diffraction patterns display diffuse powder rings (Fig. 2B). The d -values and ring-pattern structure indicate that aggregates consist of randomly oriented, finely crystalline sphalerite (ZnS). High-resolution TEM images reveal that the diameter of particles within aggregates is ~3 nm (8). Thus, ~3- μm -diameter aggregates consist of about a

¹Department of Geology and Geophysics, University of Wisconsin–Madison, 1215 West Dayton Street, Madison, WI 53706, USA. ²Diversions Scuba, Madison, WI 53705, USA. ³Department of Physics, University of Wisconsin–Madison, 1150 University Avenue, Madison, WI 53706, USA. ⁴Argonne National Laboratory, Argonne, IL 60439, USA. ⁵Australian Geological Survey Organisation, GPO Box 378, Canberra ACT 2601, Australia.

*To whom correspondence should be addressed. E-mail: jill@geology.wisc.edu